DOI:10.28974/idojaras.2026.2.3

IDŐJÁRÁS

Quarterly Journal of the HungaroMet Hungarian Meteorological Service
Vol. 130, No. 2, January – March, 2026, pp. 135–150

Study on the performance of WRF 4DVAR with GSMaP_NOW rainfall assimilation in forecasting heavy rainfall over the Maritime Continent

Achmad Fahruddin Rais[1*], **Giarno**[2], **Sayful Amri**[2], **Muflihah**[3], **Nurtiti Sunusi**[4], **Didiharyono**[5], **Agustina Rachmawardani**[6], **Hariyanto**[6], **Bono Pranoto**[1], **Muhammad Syamsudin**[3], and **Bagus Satrio Utomo**[3]

[1]*Research Centre of Limnology and Water Resource, Research and Innovation Agency, Indonesia*

[2]*Climatology Study Program, School of Meteorology, Climatology and Geophysics, Indonesia*

[3]*Balai Besar Wilayah IV, Agency for Meteorology, Climatology and Geophysics, Indonesia*

[4]*Departemen of Statistic, Hasanuddin University, Indonesia*

[5]*Research Center for Computing, Research and Innovation Agency, Indonesia*

[6]*Instrumentation Study Program, School of Meteorology, Climatology and Geophysics, Indonesia*

**Corresponding author E-mail: achm050@brin.go.id*

(Manuscript received in final form on December 25, 2025)

Abstract— This study evaluated the performance of the Weather Research and Forecasting (WRF) model with Four-Dimensional Variational (4DVar) data assimilation using the Global Satellite Mapping of Precipitation (GSMaP_NOW). Several verification metrics, including the root mean square error (RMSE), bias Score, equitable threat score (ETS), - fractional bias score (FBS), and fractional skill score (FSS) were employed in the assessment. The results demonstrated that 4DVar improved the accuracy of vertical velocity and specific humidity predictions at mid and upper levels, as well as the enhanced heavy rainfall forecasting. Spatially, 4DVar was able to increase specific humidity and vertical velocity in lowland areas, leading to higher rainfall in those regions. Future studies should investigate the assimilation of additional conventional and satellite observations to further enhance forecast accuracy.

Key-words: 4DVar, GSMaP_NOW, Maritime Continent, WRF, rainfall

1. Introduction

The Maritime Continent (MC) is recognized as the region with the highest precipitation in the tropics, mainly due to its status as the area with the longest coastline in the world (*Yamanaka*, 2016). Extensive forests and mountainous terrains also significantly contribute to rainfall generation across the MC (*Ruppert* and *Chen*, 2020). This region's diurnal cycle over land is particularly pronounced (*Argüeso et al.*, 2020). Differential solar heating across land and sea surfaces induces local pressure gradients that drive sea–land breeze circulations. These circulations, combined with orographic lifting and nocturnal downdrafts, constitute the area's primary mechanisms for rainfall formation (*Qian*, 2008). Positioned between the Pacific and Indian Oceans, the weather dynamics of the MC substantially influence the global climate system (*Chen et al.*, 2023).

Heavy precipitation in this region has multidimensional impacts, encompassing environmental, social, economic, and public health domains. Ecologically, extreme rainfall can disrupt ecosystem balance by triggering soil erosion, habitat degradation, and altered hydrological patterns that often result in flash floods (*Trenberth*, 2005; *Li et al.*, 2019). In agriculture, intense rainfall damages crops and reduces yields, particularly for sensitive commodities such as maize, sugarcane, and turmeric, and increases the economic vulnerability of smallholder farmers (*Guo* and *Chen*, 2022; *Muthiah et al.*, 2025). The socio-economic repercussions also extend to infrastructure and construction, where poor drainage systems and rainfall-induced landslides can lead to structural damage and disrupt essential public services (*Jiang* and *Tan*, 2021). Rapid urbanization amplifies flood risks in urban areas by increasing surface runoff volume and shortening rainfall concentration time, thereby intensifying the likelihood of localized flooding (*Huang et al.*, 2011; *Sahoo et al.*, 2020). From a public health perspective, high precipitation is linked to rising waterborne diseases, such as diarrhea, particularly in communities lacking adequate sanitation infrastructure (*Carlton et al.*, 2014). Irregular and intense rainfall events further affect food security and clean water supply, exacerbating social inequalities in disaster-prone regions.

Rainfall forecasting in tropical regions presents greater challenges than in the subtropics, due to its lower accuracy (*Haiden et al.*, 2012). This discrepancy stems from the complexity of tropical atmospheric systems and their connections to both local convection and large-scale equatorial waves, such as Convectively Coupled Equatorial Waves (CCEWs) and the Madden–Julian Oscillation (MJO), which remain difficult to represent accurately in numerical weather prediction (NWP) models (*Zhu et al.*, 2014; *Gehne et al.*, 2022). Nevertheless, the tropics exhibit longer predictability horizons, attributed to the dominant role of equatorial waves, which help prolong forecast skill and are more resilient to error growth than baroclinic disturbances in mid-latitudes (*Judt*, 2020). Additionally, NWP forecasts in the tropics rely heavily on convective parameterization, which introduces further uncertainty (*Selz* and *Craig*, 2015).

The Four-Dimensional Variational Data Assimilation (4DVar) method has enhanced precipitation forecast accuracy for up to 10 days ahead (*Lopez*, 2013). 4DVar enables the assimilation of multitemporal observations, consistent with the model dynamics, leading to more realistic atmospheric state estimations (*Tiwari* and *Kumar*, 2022). The longer the observational period assimilated, the greater the increase in the forecast accuracy (*Trémolet*, 2006).

Numerous studies have explored the integration of 4DVar with remote sensing. Some researchers have assimilated radar data into models (*Ban et al.*, 2017; *Tai et al.*, 2020; *Thiruvengadam et al.*, 2020; *Syafitri* and *Sari*, 2021), while others have focused on satellite data (*Lin et al.*, 2017; *Pan et al.*, 2017; *Yi et al.*, 2018; *Wu et al.*, 2020; *Zhang et al.*, 2020; *Gopalakrishnan* and *Chandrasekar*, 2022; *Vourlioti et al.*, 2022; *Wang et al.*, 2023; *Ren et al.*, 2024; *Patel et al.*, 2025). Radar-based rainfall estimation is more reliable than satellite data (*Jiang et al.*, 2019) and provides higher resolution (*Tesfagiorgis et al.*, 2011). However, weather radar systems are limited in terms of coverage area. For regions not covered by radar, the assimilation of satellite data provides an alternative to improve forecast accuracy. One such product is GSMaP, which offers a latency of approximately one hour, faster than the IMERG product of NOAA (*P. Neeck* and *Oki*, 2018). While the assimilation of GSMaP data into NWP models for precipitation forecasting has been limited, *Kumar et al.* (2014) are among the few to investigate the impact of assimilating GSMaP rainfall data using WRF 4DVar.

This study aims to assess the impact of assimilating GSMaP data with WRF 4DVar on forecasting heavy rainfall in the MC. This research will focus on central Sulawesi, located in the heart of the MC. The study will consider six heavy rainfall events resulting in flooding and landslides, causing loss of life and material damage (BNPB, 2024). These six events occurred on July 12, 2020; October 3, 2021; October 29, 2021; October 18, 2022; May 16, 2023; and May 2, 2024.

2. Materials and methods

As the primary reference for this study, we use 139 rainfall gauges operated by the Indonesian Agency for Meteorology, Climatology and Geophysics (BMKG), symbolized as a black circle in *Fig. 1*. Weather station measurements serve as the primary source of rainfall observations over land (*Barlow et al.*, 2019). The FNL (Final Analysis) data are provided by the NOAA (*UCAR*, 2015a). It is used as the spin-up time data for the WRF-ARW model for 12 hours. Additionally, we utilize the GFS (Global Forecast System) from NOAA (*UCAR*, 2015b) as the boundary condition forecast. For the assimilated data, we employ Global Satellite Mapping of Precipitation NOW (GSMaP_NOW), which is accumulated every 6 hours.

In *Fig. 1*, the study area is central Sulawesi, marked with a red line. Domain 1 of WRF covers most of Sulawesi, with spatial and temporal output resolutions of 10 km and 3 hours, respectively, illustrated as a purple box. Domain 2

encompasses the study area with spatial and temporal output resolutions of 2 km and 1 hour, respectively, marked with a black box. The vertical levels for both domains are set to 34, which aligns with the vertical levels of the GFS.

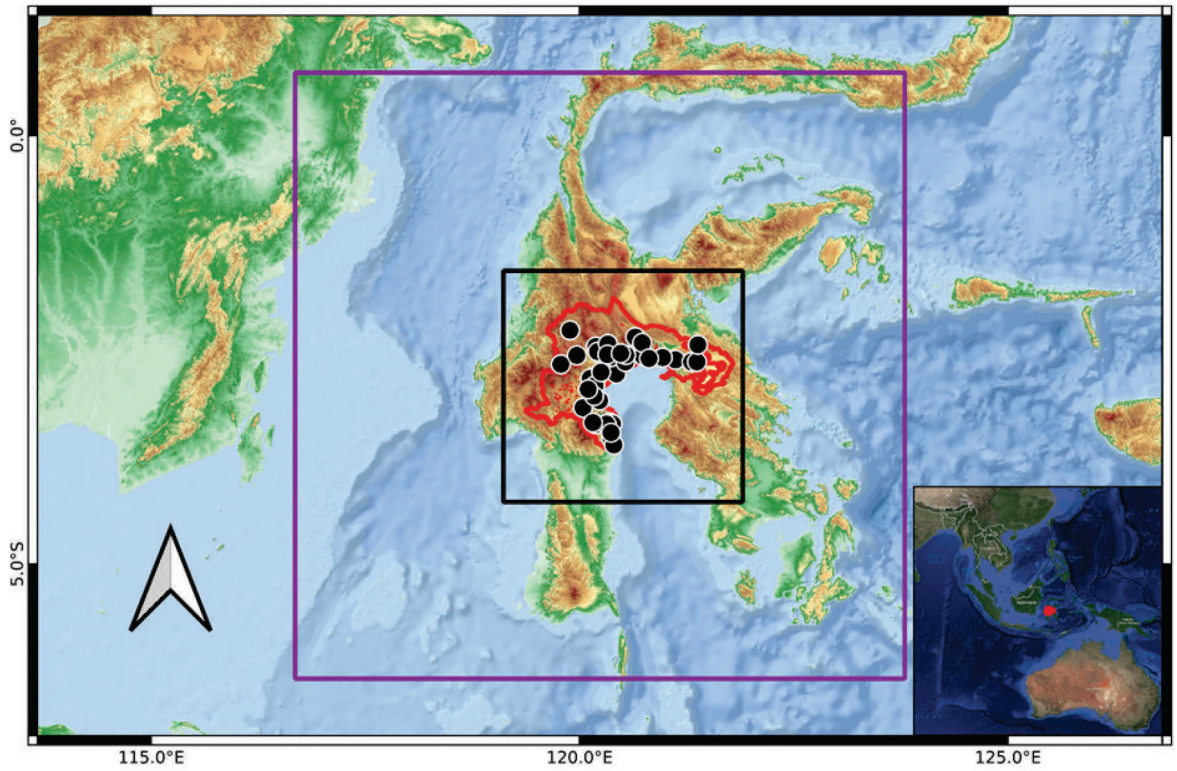

Fig. 1. WRF-ARW domain 1 (purple box), domain 2 (black box), study area (red line), and rain gauges (black circles)

For this study, we employ tropical-specific physical parameterizations (*Table 1*), which include the WRF Single Moment 6-Class (WSM6) microphysics scheme, the more recent Tiedtke scheme for cumulus convection, the Rapid Radiative Transfer Model for Global Circulation Models (RRTMG) for both shortwave and longwave radiations, and the Yonsei University (YSU) scheme for the planetary boundary layer. Notably, the WSM6 scheme includes graupel production in the microphysical process (*Hong* and *Lim*, 2006), distinguishing it from the WSM5 scheme (*Lim* and *Hong*, 2005). The more recent Tiedtke scheme calculates cloud and ice mixing ratios, momentum tendencies, and shallow convection (*Skamarock et al.*, 2019). This scheme has been shown to capture the fundamental characteristics of the marine boundary layer structure and low clouds (*Zhang et al.*, 2011) and provide improved diurnal precipitation simulations (*Sun* and *Bi*, 2019). Additionally, the RRTMG scheme offers more accurate radiation forcing results, especially for high-resolution computations (*Iacono et al.*, 2008).

Table 1. WRF-ARW configuration for domain 1 and domain 2

Configuration	Domain 1	Domain 2
Temporal resolution	3 h	1 h
Spatial resolution	10 km	2 km
Vertical level	34	34
Parameterization	*Tropical*	*Tropical, Cu=0*

The WRF model is run for non-assimilation (NONDA) and 4DVar assimilation (DA) scenarios. NONDA uses FNL data at 12 UTC and 18 UTC for a 12-hour spin-up time, followed by forecasts up to t+24 hours. In contrast, DA assimilates 3-hour accumulated GSMaP data at 18 UTC and 00 UTC, with assimilation performed within Domain 1 (*Fig. 2*).

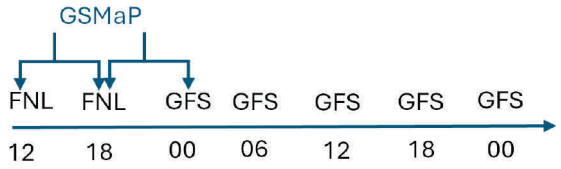

Fig. 2. Timeline of WRF.

Several WRF output variables will be analyzed, including precipitation, specific humidity, temperature, and wind. Precipitation is the sum of non-convective rainfall (RAINNC) and shallow cumulus rainfall (RAINSH). Specific humidity (Q) is calculated from the water vapor mixing ratio (r) using the formula (*Stull*, 2020):

$$Q = \frac{r}{1+r} \tag{1}$$

The DA and NONDA model forecasts will be evaluated against ERA5 reanalysis data for specific humidity, temperature, and vertical velocity using the root mean square error (RMSE) metric. ERA5 is used as the reference because in-situ sounding observations are unavailable in the study area, and several researchers – such as *Kumar et al.* (2014), *Xie et al.* (2018), and *Zheng et al.*(2023) – have employed ERA5 in similar contexts. RMSE measures the average error between the predicted values from the model and the actual observed values (*James et al.*, 2013). For assessing the accuracy and bias of the rainfall forecasts, DA and NONDA rainfall predictions will be tested against the rain gauge data using the bias score (*Hayashi et al.*, 2008; *Gao et al.*, 2021; *Syafitri* and *Sari*, 2021) and equitable threat score (ETS) (*Hayashi et al.*, 2008; *Mohanty et al.*, 2012; *Kumar et al.*, 2014; *Wu et al.*, 2020; *Rakesh* and *Kutty*, 2021; *Wang et al.*, 2023). Rainfall evaluation will also use nine surrounding grids with the fractional bias score (FBS) and fractional skill score (FSS) methods (*Ban et al.*, 2017; *Wu et al.*, 2020; *Wang et al.*, 2023). FBS and FSS are used to quantitatively assess the spatial skill of rainfall forecasts, particularly when differences between experiments are not visually distinct (*Roberts* and *Lean*, 2008).

3. Results and discussion

3.1. Observation analysis

On October 18, 2022 (*Fig. 3d*) and May 2, 2024 (*Fig. 3f*), the maximum rainfall occurred in the mountainous regions, as indicated by the black 500 m elevation contours. The maximum rainfall was observed in the lowlands on other dates (*Figs. 3a-c* and *3e*). The maximum rainfall is localized, with no significant rainfall observed in the surrounding areas, except on July 12, 2020 (*Fig. 3a*). This highlights the necessity of high-resolution models to accurately predict the spatial distribution of rainfall. Furthermore, extreme rainfall in these lowland areas could not be adequately simulated using only the WRF NONDA model in the study by *Yulihastin et al.* (2021).

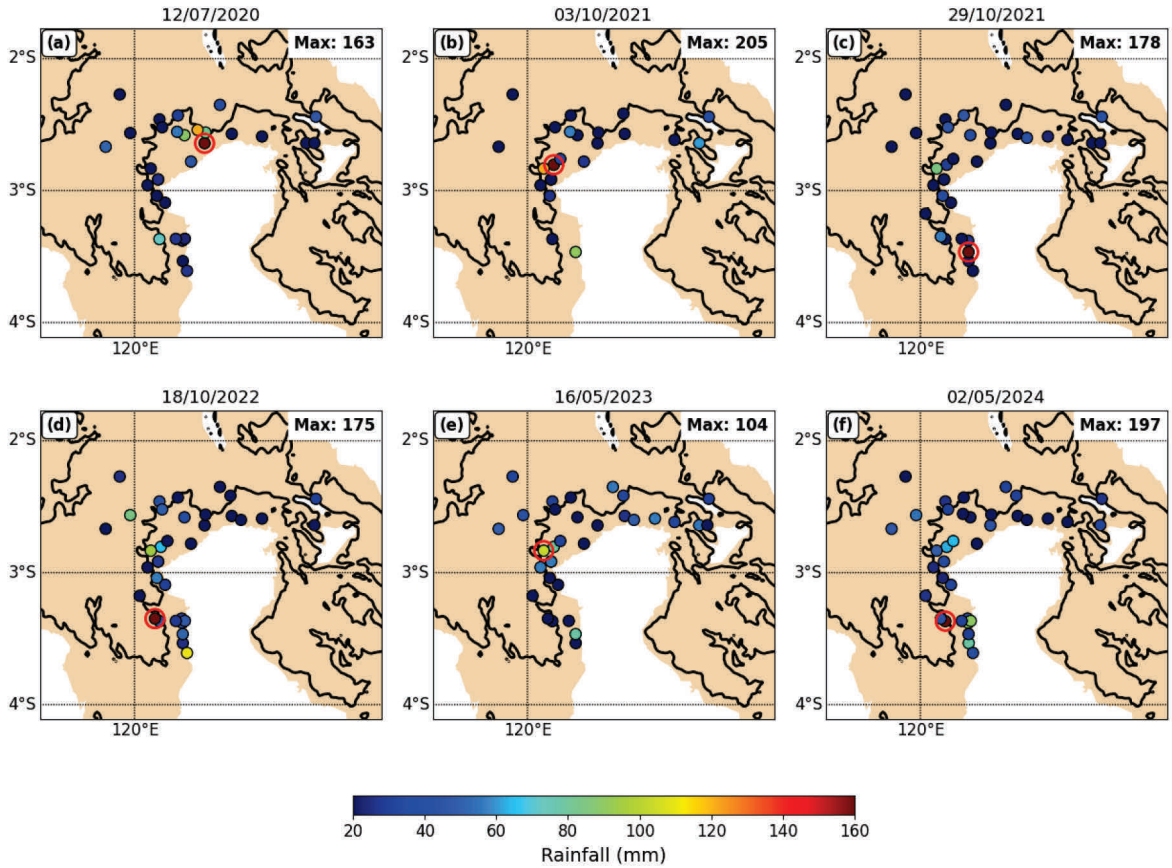

Fig. 3. 24-hour rainfall accumulation of gauges for six heavy rainfall events. The red circles are maximum rainfall locations. The black lines represent the 500 m elevation contours, and the light brown shaded area denotes the island of Sulawesi.

3.2. *Specific humidity, temperature, and vertical velocity*

Fig. 4 displays the RMSE of DA and NONDA against ERA5. The RMSE of specific humidity for DA is larger than that of NONDA in the low level at 00 UTC and 06 UTC. In comparison, the RMSE of specific humidity for DA is smaller in the middle and upper layers between 06 UTC and 18 UTC (*Fig. 4a*). In the middle layer at 00 UTC (*Fig. 4b*), the RMSE of temperature for DA is also higher than for NONDA. In contrast, *Fig. 4c* shows that the RMSE of vertical velocity for DA is smaller than NONDA in the low level at 06 UTC and in the middle and upper layers at 12 UTC. The decrease in RMSE of specific humidity in the low level and the increase in RMSE of temperature in the middle layer for DA compared to NONDA are also simulated in the study by (*Xie et al.*, 2018), which used 3DVar assimilation of AMSU-A and MHS radiation. Additionally, DA rainfall assimilation reduces the RMSE of specific humidity when compared to conventional observation assimilation at the 1000 hPa layer (*Wang et al.*, 2023).

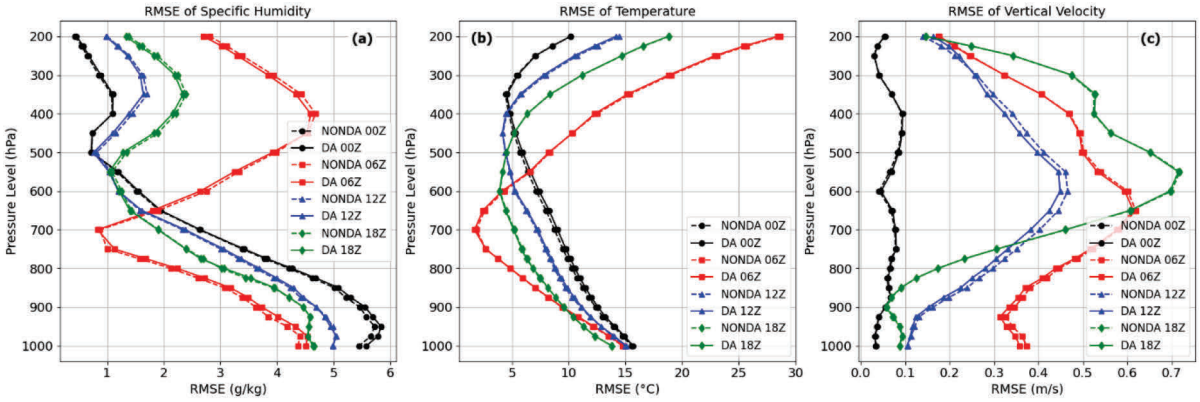

Fig. 4. RMSE DA and NONDA against ERA5 for (a) specific humidity, (b) temperature, and (c) vertical velocity.

In the time section of *Fig. 5a*, the specific humidity (*Q*) for DA reaches its maximum between 06 UTC and 08 UTC, with values approaching 16 g/kg, which is lower than NONDA. The *Q* for DA in the low to mid-levels (1–5 km) becomes larger after 12 UTC, which is consistent with the findings of Pan et al. (2022). At mid to upper levels (6–9 km), the *Q* in DA is higher than in NONDA from 01 to 07 UTC, but then becomes lower starting at 08 UTC.

The temperature (*T*) at the low level for DA shows slight temporal variation (*Fig. 5b*), as the diurnal temperature variation in the tropics is much smaller than in the subtropics (*Riehl*, 1979). At low levels (1–4 km), the *T* of DA is only higher than NONDA between 00 UTC and 03 UTC, after which it becomes lower. At mid-levels (4–7 km), the *T* of DA exceeds that of NONDA starting from 06 UTC, although the difference remains small. At upper levels (9–12 km), the T of DA is higher than NONDA between 01 and 05 UTC.

In *Fig. 5c*, the vertical velocity (*W*) in the low level for DA is positive starting from 00 UTC and extends to the upper layers by 06 UTC. This upward motion weakens after 12 UTC. Compared to NONDA, positive changes are observed in the middle and upper layers, especially at 07 UTC and 09–14 UTC. In contrast, at the low level, the *W* for DA is lower than for NONDA, except at 07 UTC when the *W* of DA exceeds that of NONDA. *Mohanty et al*. (2012), *Narasimha Rao et al.* (2020), and *Pan et al.* (2022) also observed an increase in vertical velocity values.

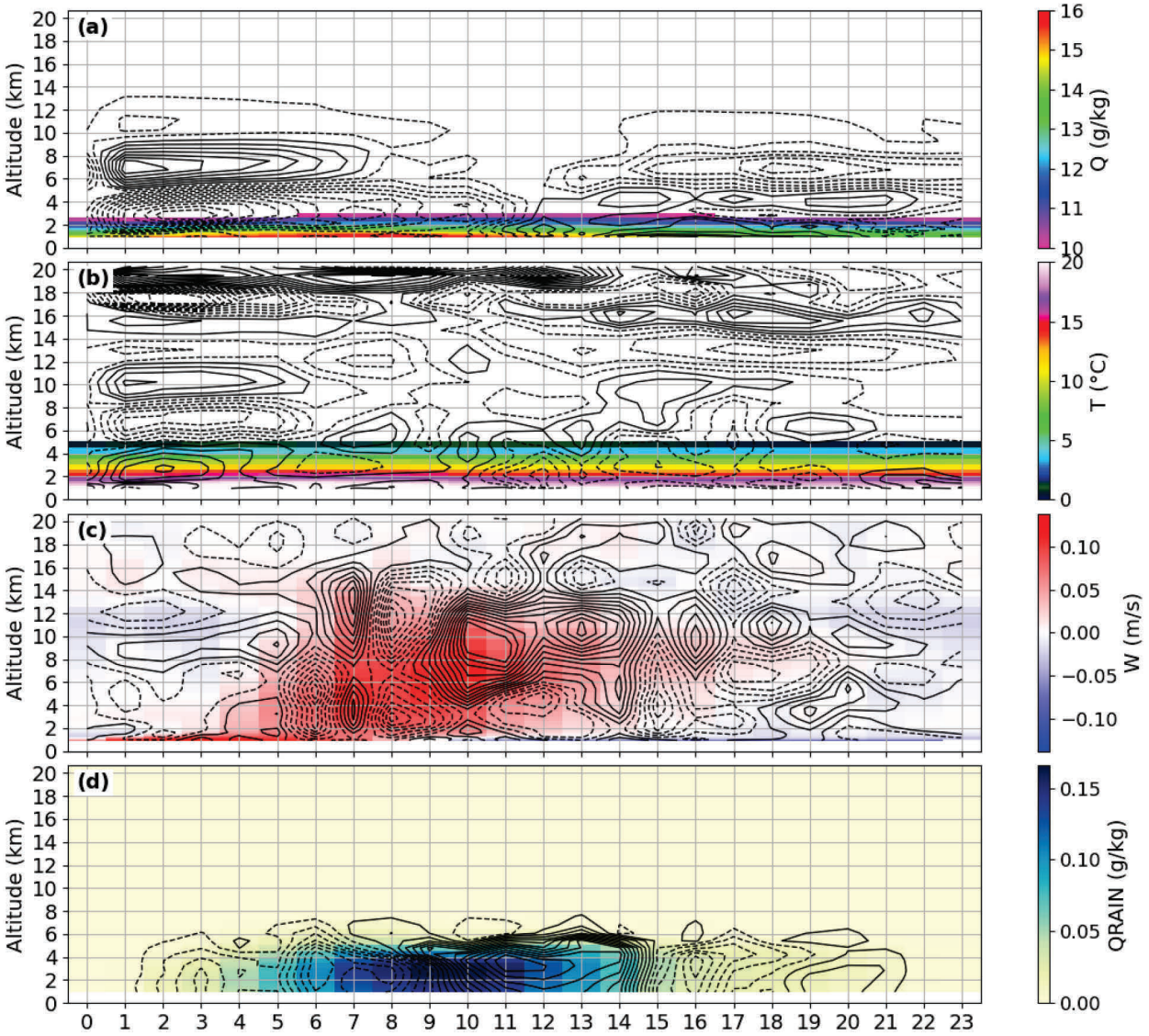

Fig. 5. Time–height section of the DA composite (shading) and DA–NONDA difference (contours) for (a) specific humidity, (b) temperature, (c) vertical velocity, and (d) rainwater mixing ratio. Solid contours are for positive values and dashed contours are for negative values.

Fig. 5d shows that the rainwater mixing ratio (*QRAIN*) reaches its maximum between 07 and 11 UTC, with values confined below 4 km altitude. This peak in

QRAIN occurs prior to the maximum *Q* and coincides with the maximum *W*. The observed lag time reflects the process of water vapor converting into raindrops. The coincidence indicates the direct influence of strong vertical velocity on *QRAIN*. Compared to NONDA, *QRAIN* in the DA experiment is higher between 10 and 14 UTC, coinciding with enhanced *W* at mid and upper levels.

At the low level, ΔQ is generally negative at 00 and 06 UTC (*Fig. 6a-b*), except for some areas in the mountainous region where it becomes positive at 06 UTC. The most significant increase in *Q* for DA occurs in the western region, covering both the lowlands and mountainous areas at 12 UTC (*Fig. 6c*), and is limited to the mountainous areas at 18 UTC (*Fig. 6d*). The increase in *T* of DA is mostly concentrated over mountainous regions at 00 UTC (Fig. 6e), but becomes negative at 06 UTC (*Fig. 6f*). The reduction in ΔT at 12 UTC intensifies due to evaporative cooling caused by rainfall (*Fig. 6g–h*). Although the general pattern of ΔW is negative, the spatial distribution of ΔW shows positive values in the mountains at 06 UTC (*Fig. 6j*) and in the lowlands at 12 UTC (*Fig. 6k*). No significant changes in *W* are observed at 00 UTC (*Fig. 6i*) and 18 UTC (*Fig. 6l*). *Xiong et al.* (2020) also observed the same general pattern, where topography influences the assimilation in WRF.

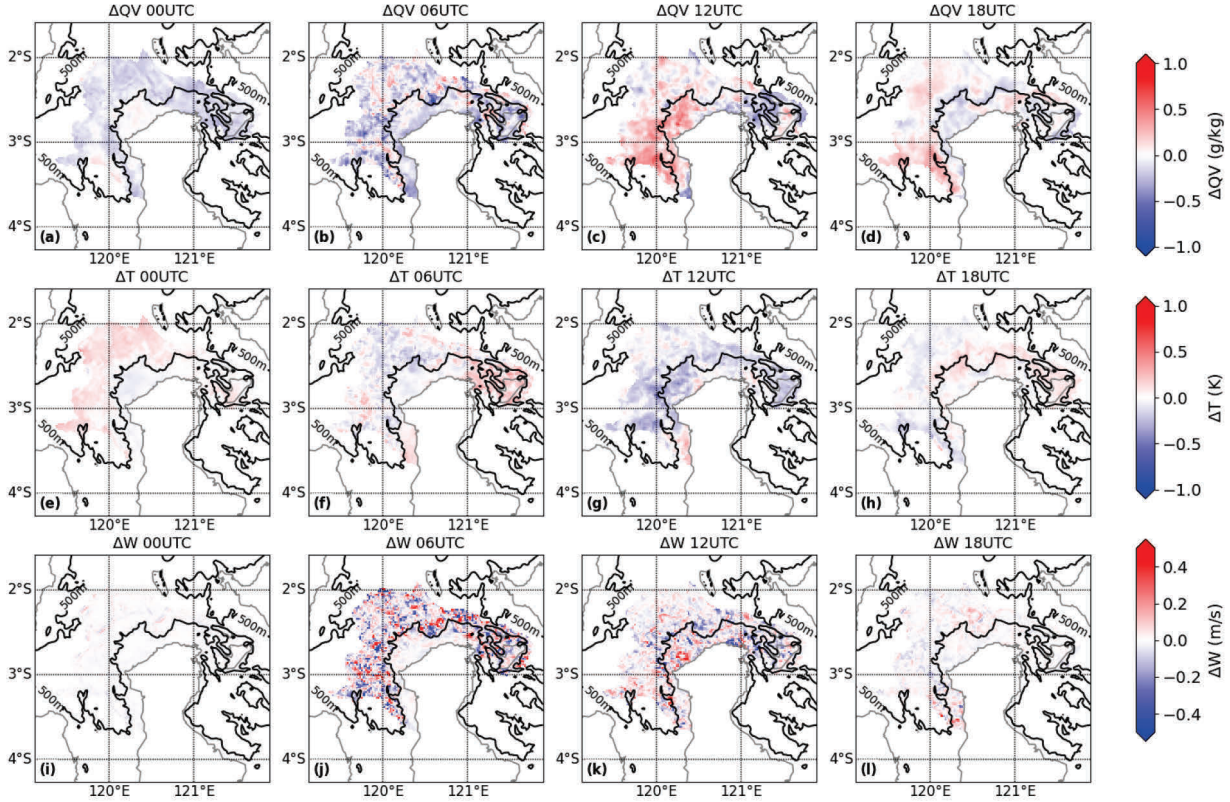

Fig. 6. Composite of DA–NONDA differences at low levels for (a–d) specific humidity, (e–h) temperature, and (i–l) vertical velocity. Contours represent elevations at 500 m.

3.3. Rainfall

Fig. 7a shows that DA and NONDA predict rainfall as underestimated, with a bias score of less than 1. DA predicts higher rainfall than NONDA in 10–40 mm, 80 mm, and 130–140 mm, while it predicts lower rainfall in 50 mm, 100 mm, and 120 mm. The ETS for both DA and NONDA is generally very small, with accuracy improvements in 20-30 mm and 60-80 mm, and DA being worse in the 40-50 mm (*Fig. 7b*). Although the ETS for DA is small, similar to the smaller rainfall ETS in tropical regions compared to subtropical areas (*Hayashi et al.*, 2008), DA generally improves the prediction of heavy rainfall, as found in the research by Dhanya and Chandrasekar using WRF 3DVar (*Dhanya and Chandrasekar*, 2016).

Considering nearby grids, the FBS for DA is less than 1, indicating that the predicted rainfall for DA is lower than the observed rainfall. The FBS for DA is lower than for NONDA in the 60-80 mm rainfall range, but higher in the 10-40 mm range (*Fig. 7c*). In *Fig. 7d*, the FSS for DA is greater than 0.6 only up to the 20 mm threshold. The FSS for DA is smaller than for NONDA in the 10-40 mm rainfall range, but larger in the 60-80 mm rainfall range.

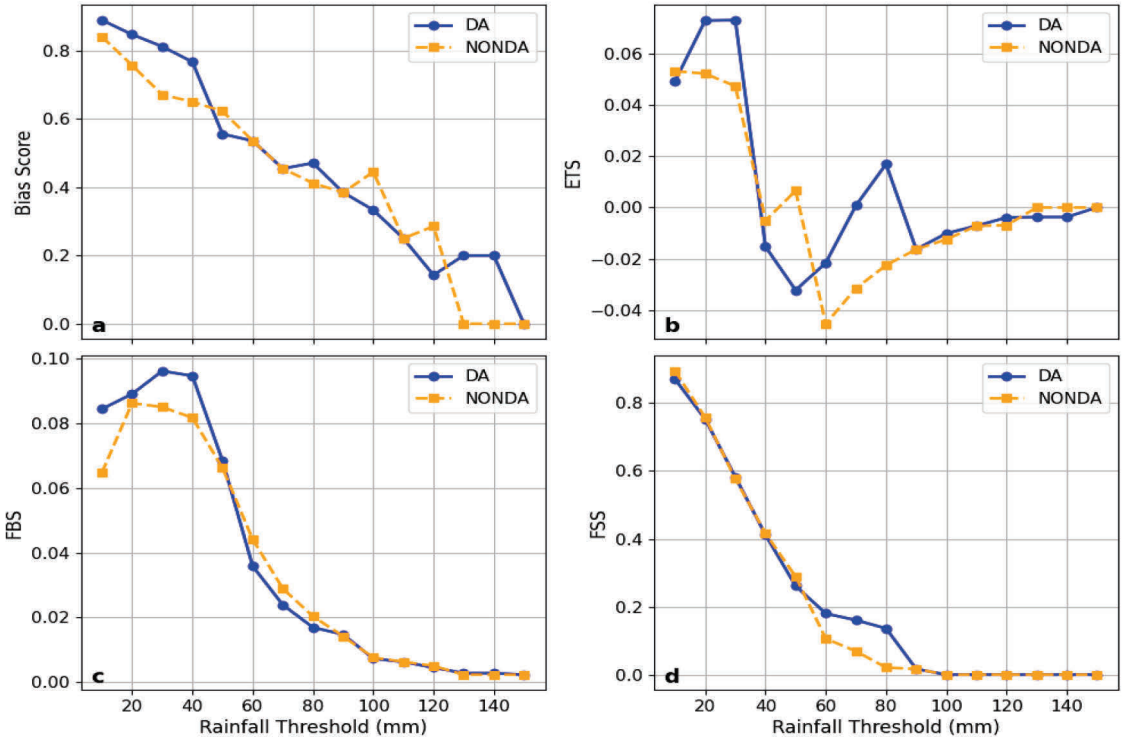

Fig. 7. Daily rainfall verification scores at several thresholds: (a) bias score, (b) equitable threat score, (c) fractional bias store, and (d) fractional skill score.

Fig. 8 shows that the mean rainfall predicted over the study area by the DA model exceeds that of the NONDA model during the spin-up period. This suggests a significant impact of satellite rainfall assimilation in the initial hours post-analysis. The forecasted rainfall in DA peaks more gradually than in NONDA, leading to a negative DA-NONDA difference until 09 UTC, after which it becomes positive. Both models exhibit the same start and end times for rainfall. Since the values represent spatial averages over the study area, slight differences in DA–NONDA rainfall may correspond to substantial discrepancies at localized scales.

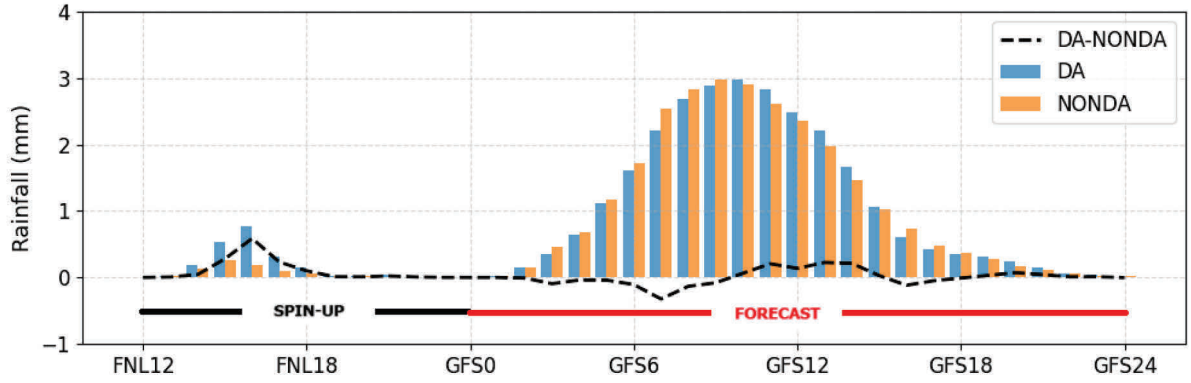

Fig. 8. Composite of area-averaged diurnal rainfall of DA and NONDA.

At 00 UTC, rainfall in both DA (*Fig. 9a*) and NONDA (*Fig. 9e*) remains below 1 mm/h. By 06 UTC, rainfall in DA (Fig. 9b) and NONDA (*Fig. 9f*) is concentrated over the mountainous regions. At 12 UTC, rainfall in both models (*Fig. 9c* and *Fig. 9g*) extends across the entire study area, including the lowlands and mountains. DA predicts greater rainfall in the lowlands at 12 UTC (*Fig. 9k*) compared to NONDA. This enhancement is attributed to increased Q and stronger W in the lowlands. By 18 UTC, rainfall diminishes sharply in both DA (*Fig. 9d*) and NONDA (*Fig. 9h*). This diurnal rainfall pattern aligns with typical conditions observed in the MC, as *Sakaeda et al.* (2020) and *Cui* and *Pu* (2023) reported. The improved lowland rainfall prediction by the DA experiment demonstrates the effectiveness of GSMaP assimilation in enhancing model performance, particularly in regions often underestimated in NONDA runs. This result highlights the potential of GSMaP assimilation as a reliable alternative to weather radar assimilation, which has already been shown to improve forecast accuracy (*Ban et al.*, 2017; *Tai et al.*, 2020; *Thiruvengadam et al.*, 2020; *Syafitri* and *Sari*, 2021). Furthermore, GSMaP assimilation offers a practical solution for areas lacking radar coverage, making it especially valuable for operational forecasting in data-sparse regions.

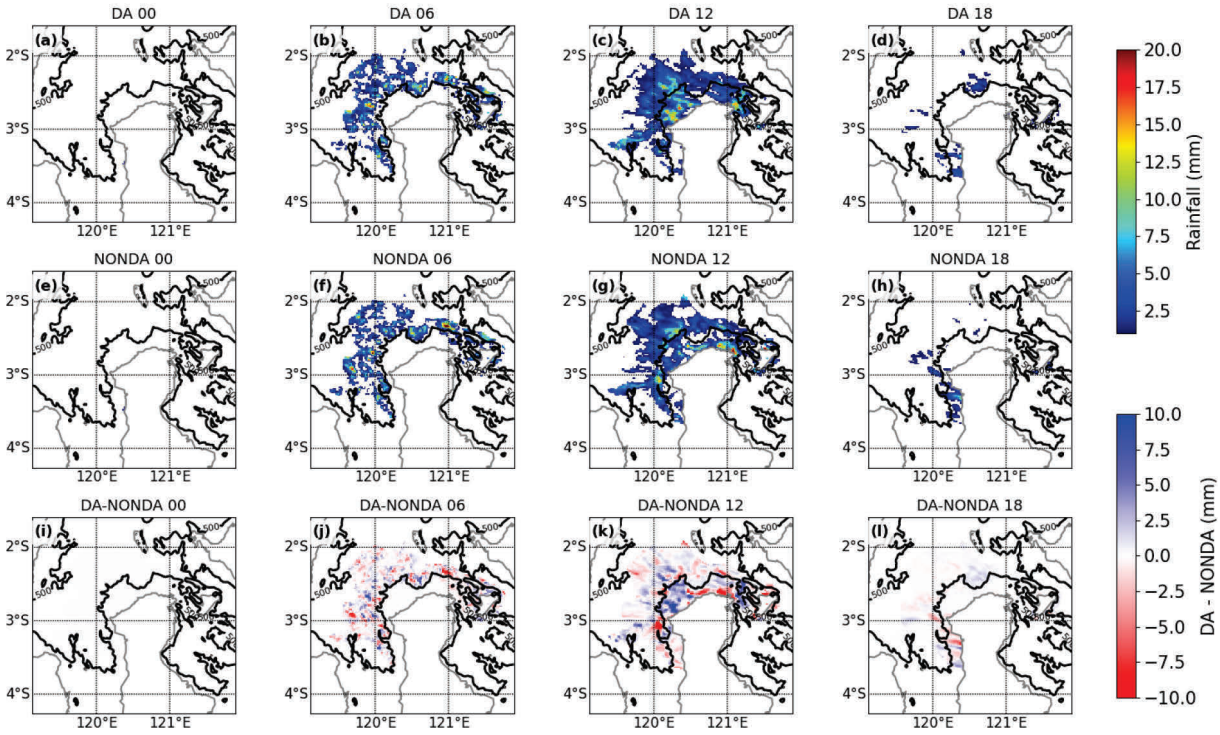

Fig. 9. Rainfall composite of DA (a-d), NONDA (e-h), and DA-NONDA (i-l). Contours represent elevations at 500 m.

4. Conclusions

This study examines the performance of WRF 4DVAR with GSMaP rainfall assimilation compared to a non-assimilated WRF at a 2 km resolution in forecasting six heavy rainfall events that led to floods and landslides in the Maritime Continent. The findings indicate that DA improves the accuracy of vertical velocity and specific humidity predictions, particularly in the middle and upper atmospheric layers. DA shows lower specific humidity values at lower levels and higher values at mid-to-upper levels. While temperature differences between DA and NONDA are minimal, DA slightly increases temperatures at mid and upper levels and exhibits more pronounced upward vertical velocity at these levels. DA predicts higher rainwater mixing ratios, which correspond to higher vertical velocity. Additionally, DA improves the accuracy of heavy rainfall predictions, enhancing rainfall forecasting, particularly in lowland regions, in line with the specific humidity and vertical velocity patterns.

References

Argüeso, D., Romero, R., and *Homar, V.*, 2020: Precipitation features of the maritime continent in parameterized and explicit convection models. *Journal of Climate*, *33*. https://doi.org/10.1175/JCLI-D-19-0416.1

Ban, J., Liu, Z., Zhang, X., Huang, X.Y., and *Wang, H.*, 2017: Precipitation data assimilation in WRFDA 4D-Var: implementation and application to convection-permitting forecasts over United States. *Tellus, Series A: Dynamic Meteorology and Oceanography*, *69*. https://doi.org/10.1080/16000870.2017.1368310

Barlow, M., Gutowski, W.J., Gyakum, J.R., Katz, R.W., and *Lim, Y.K.*, 2019: North American extreme precipitation events and related large-scale meteorological patterns: A review of statistical methods, dynamics, modeling, and trends. *Climate Dynamics*, *53*, 1841–1863. https://doi.org/10.1007/s00382-019-04958-z

Carlton, E.J., Eisenberg, J.N.S., Goldstick, J., Cevallos, W., Trostle, J., and *Levy, K.*, 2014: Heavy rainfall events and diarrhea incidence: The role of social and environmental factors. *American Journal of Epidemiology*, *179*. https://doi.org/10.1093/aje/kwt279

Chen, C., Sahany, S., Moise, A.F., Chua, X.R., Hassim, M.E., Lim, G., and *Prasanna, V.*, 2023: ENSO–Rainfall Teleconnection over the Maritime Continent Enhances and Shifts Eastward under Warming. *Journal of Climate*, *36*. https://doi.org/10.1175/JCLI-D-23-0036.1

Cui, Z., and *Pu, Z.*, 2023: The Use of Regional Data Assimilation to Improve Numerical Simulations of Diurnal Characteristics of Precipitation during an Active Madden–Julian Oscillation Event over the Maritime Continent. *Remote Sensing*, *15*. https://doi.org/10.3390/rs15092405

Dhanya, M., and *Chandrasekar, A.*, 2016: Impact of variational assimilation using multivariate background error covariances on the simulation of monsoon depressions over India. *Annales Geophysicae*, *34*. https://doi.org/10.5194/angeo-34-187-2016

Gao, S., Yu, H., Ren, C., Liu, L., and *Min, J.*, 2021: Assimilation of Doppler Radar Data with an Ensemble 3DEnVar Approach to Improve Convective Forecasting. *Advances in Atmospheric Sciences*, *38*. https://doi.org/10.1007/s00376-020-0081-z

Gehne, M., Wolding, B., Dias, J., and *Kiladis, G.N.*, 2022: Diagnostics of Tropical Variability for Numerical Weather Forecasts. *Weather and Forecasting*, *37*. https://doi.org/10.1175/WAF-D-21-0204.1

Gopalakrishnan, D., and *Chandrasekar, A.*, 2022: The sensitivity of the WRF-4DVar data assimilation system to the control variables: A study on heavy rainfall events over India. *Dynamics of Atmospheres and Oceans*, *99*, 101304. https://doi.org/10.1016/j.dynatmoce.2022.101304

Guo, J., and *Chen, J.*, 2022: The Impact of Heavy Rainfall Variability on Fertilizer Application Rates: Evidence from Maize Farmers in China. *International Journal of Environmental Research and Public Health*, *19*. https://doi.org/10.3390/ijerph192315906

Haiden, T., Rodwell, M.J., Richardson, D.S., Okagaki, A., Robinson, T., and *Hewson, T.*, 2012: Intercomparison of global model precipitation forecast skill in 2010/11 using the SEEPS score. *Monthly Weather Review*, *140*. https://doi.org/10.1175/MWR-D-11-00301.1

Hayashi, S., Aranami, K., and *Saito, K.*, 2008: Statistical Verification of Short Term NWP by NHM and WRF-ARW with 20 km Horizontal Resolution around Japan and Southeast Asia *4*, 133–136.

Hong, S.-Y., and *Lim, J.-O.J.*, 2006: The WRF Single-Moment 6-Class Microphysics Scheme (WSM6). *Journal of Korean Meteorlogy 42(2)*, 129–151..

Huang, J.J., Gan, Y.Q., Miao, S.X., Wu, J.Q., Yang, L., Hua, M., Min, W., Zhao, L.H., and *Fang, Q.*, 2011: A preliminary study of the evaluation index system for geo-environment regionalization in Jiangsu. *Geol China*, *38*. https://doi.org/10.3969/j.issn.1000-3657.2011.06.020

Iacono, M.J., Delamere, J.S., Mlawer, E.J., Shephard, M.W., Clough, S.A., and *Collins, W.D.*, 2008: Radiative forcing by long-lived greenhouse gases: Calculations with the AER radiative transfer models. *Journal of Geophysical Research Atmospheres*, *113*. doi:10.1029/2008JD009944

James, G., Witten, D., Hastie, T., and *Tibishirani, R.*, 2013: *An Introduction to Statistical Learning with Applications in R (older version)*, Springer Texts in Statistics.

Jiang, Q., Li, W., Wen, J., Fan, Z., Chen, Y., Scaioni, M., and *Wang, J.*, 2019: Evaluation of satellite-based products for extreme rainfall estimations in the eastern coastal areas of China. *Journal of Integrative Environmental Sciences*, *16*, 191–207. https://doi.org/10.1080/1943815X.2019.1707233

Jiang, W., and *Tan, Y.*, 2021: Heavy rainfall-related excavation failures in China during 1994 to 2018: An overview. *Engineering Failure Analysis*,. doi:10.1016/j.engfailanal.2021.105695

Judt, F., 2020: Atmospheric predictability of the tropics, middle latitudes, and polar regions explored through global storm-resolving simulations. *Journal of the Atmospheric Sciences*, *77*. https://doi.org/10.1175/JAS-D-19-0116.1

Kumar, P., Kishtawal, C.M., and *Pal, P.K.*, 2014: Impact of satellite rainfall assimilation on weather research and forecasting model predictions over the Indian region. *Journal of Geophysical Research*, *119*. https://doi.org/10.1002/2013JD020005

Li, L., Zheng, Z., Biederman, J.A., Xu, C., Xu, Z., Che, R., Wang, Y., Cui, X., and *Hao, Y.*, 2019: Ecological responses to heavy rainfall depend on seasonal timing and multi-year recurrence. *New Phytologist*, *223*. https://doi.org/10.1111/nph.15832

Lim, J.O.J., and *Hong, S.Y.*, 2005: Effects of bulk ice microphysics on the simulated monsoonal precipitation over east Asia. *Journal of Geophysical Research Atmospheres*, *110*, 1–16. https://doi.org/10.1029/2005JD006166

Lin, L.F., Ebtehaj, A.M., Flores, A.N., Bastola, S., and *Bras, R.L.*, 2017: Combined assimilation of satellite precipitation and soil moisture: A case study using TRMM and SMOS data. *Monthly Weather Review*, *145*, 4997–5014. https://doi.org/10.1175/MWR-D-17-0125.1

Lopez, P., 2013: Experimental 4D-var assimilation of SYNOP rain gauge data at ECMWF. *Monthly Weather Review*, *141*. https://doi.org/10.1175/MWR-D-12-00024.1

Mohanty, U.C., Routray, A., Osuri, K.K., and *Kiran Prasad, S.*, 2012: A study on simulation of heavy rainfall events over Indian region with ARW-3DVAR modeling system. *Pure and Applied Geophysics*, *169*. https://doi.org/10.1007/s00024-011-0376-1

Muthiah, K., Arunya, K.G., Sridhar, V., and *Patakamuri, S.K.*, 2025: Heavy Rainfall Impact on Agriculture: Crop Risk Assessment with Farmer Participation in the Paravanar Coastal River Basin. *Water*,. doi:10.3390/w17050658

Narasimha Rao, N., Shekhar, M.S., and *Singh, G.P.*, 2020: Forecasting extreme precipitation event over Munsiyari (Uttarakhand) using 3DVAR data assimilation in mesoscale model. *Journal of Earth System Science*, *129*. https://doi.org/10.1007/s12040-019-1315-2

P. Neeck, S., and *Oki, R.*, 2018: Precipitation Virtual Constellation (P-VC). URL https://ceos.org/document_management/Meetings/SIT-Technical-Workshop/2015-SIT-Tech-Workshop/SITWS2015_VCWGDay_03_Presentation PVC rev d no anim.pdf (accessed 10.7.25).

Pan, X., Li, X., Cheng, G., and *Hong, Y.*, 2017: Effects of 4D-Var data assimilation using remote sensing precipitation products in a WRF model over the complex terrain of an arid region river basin. *Remote Sensing*, *9*. https://doi.org/10.3390/rs9090963

Pan, Z., Zhang, S., and *Zhang, W.*, 2022: Impact of Radar and Surface Data Assimilation on the Forecast of a Nocturnal Squall Line in the Yangtze–Huaihe River. *Atmosphere*, *13*. https://doi.org/10.3390/atmos13091522

Patel, S.S., Routray, A., Singh, V., Bhatla, R., Kumar, R., and *Surovyatkina, E.*, 2025: Evaluation of 3D-Var and 4D-Var data assimilation on simulation of heavy rainfall events over the Indian region. *Meteorological Applications*, *32*, 1–32. https://doi.org/10.1002/met.70037

Qian, J.H., 2008: Why precipitation is mostly concentrated over islands in the maritime continent. *Journal of the Atmospheric Sciences*, *65*, 1428–1441. https://doi.org/10.1175/2007JAS2422.1

Rais, A.F., Hudayat, N., and *Yunita, R.*, 2023: Accuracy improvement of merging real-time global satellite mapping of precipitation (GSMaP_NOW) and gauge: A case study of Jakarta flood on January 1, 2020. AIP, 040011. https://doi.org/10.1063/5.0181671

Rakesh, S., and *Kutty, G.*, 2021: Intercomparison of the Performance of Four Data Assimilation Schemes in a Limited-Area Model on Forecasts of an Extreme Rainfall Event Over the Uttarakhand in Himalayas. *Earth* and *Space Science*, *8*. https://doi.org/10.1029/2020EA001461

Ren, J., Huang, C., Hou, J., Zhang, Y., Ma, P., and *Yang, L.*, 2024: Impact of the combined assimilation of GPM/IMGER precipitation and Himawari-8/AHI water vapor radiance on snowfall forecasts

using WRF model and 4Dvar system. *Atmospheric Research*, *311*, 107726. https://doi.org/10.1016/j.atmosres.2024.107726

Riehl, H., 1979: *Climate* and *Weather in the Tropics*. Academic Press, London.

Roberts, N.M., and *Lean, H.W.*, 2008: Scale-selective verification of rainfall accumulations from high-resolution forecasts of convective events. *Monthly Weather Review*, *136*, 78–97. https://doi.org/10.1175/2007MWR2123.1

Ruppert, J.H., and *Chen, X.*, 2020: Island Rainfall Enhancement in the Maritime Continent. *Geophysical Research Letters*, *47*. https://doi.org/10.1029/2019GL086545

Sahoo, S.K., Himesh, S., and *Gouda, K.C.*, 2020: Impact of Urbanization on Heavy Rainfall Events: A Case Study over the Megacity of Bengaluru, India. *Pure and Applied Geophysics*, *177*. https://doi.org/10.1007/s00024-020-02624-8

Sakaeda, N., Kiladis, G., and *Dias, J.*, 2020: The diurnal cycle of rainfall and the convectively coupled equatorial waves over the maritime continent. *Journal of Climate*, *33*, 3307–3331. https://doi.org/10.1175/JCLI-D-19-0043.1

Selz, T., and *Craig, G.C.*, 2015: Simulation of upscale error growth with a stochastic convection scheme. *Geophys. Res. Lett.*, *42*, 3056–3062. doi:https://doi.org/10.1002/2016RG000538

Skamarock, W.C., Klemp, J.B., Dudhia, J., Gill, D.O., Liu, Z., Berner, J., Wang, W., Powers, J.G., Duda, M.G., Barker, D.M., and *Huang, X.-Y.*, 2019: A Description of the Advanced Research WRF Model Version 4. Boulder. https://doi.org/10.5065/1dfh-6p97

Stull, R., 2020: *Practical Meteorology :* An Algebra-based Survey of Atmospheric Science Roland. The University of British Columbia, 944 p.

Sun, B.Y., and *Bi, X.Q.*, 2019: Validation for a tropical belt version of WRF: sensitivity tests on radiation and cumulus convection parameterizations. *Atmospheric and Oceanic Science Letters*, *12*, 192–200. https://doi.org/10.1080/16742834.2019.1590118

Syafitri, J.D.I., and *Sari, F.P.*, 2021: Four-dimensional variational (4DVAR) performance test with assimilation satellite and radar data (case study of a heavy rainfall Bengkulu March 4, 2019), In: IOP Conference Series: Earth and Environmental Science. 10.1088/1755-1315/893/1/012031

Tai, S.L., Liou, Y.C., Chang, S.F., and *Sun, J.*, 2020: The heavy rainfall mechanism revealed by a terrain-resolving 4dvar data assimilation system-A case study. *Monthly Weather Review*, *148*, 2307–2330. https://doi.org/10.1175/MWR-D-19-0244.1

Tesfagiorgis, K., Mahani, S.E., Krakauer, N.Y., and *Khanbilvardi, R.*, 2011: Bias correction of satellite rainfall estimates using a radar-gauge product – a case study in Oklahoma (USA). *Hydrology and Earth System Sciences*, *15*. https://doi.org/10.5194/hess-15-2631-2011

Thiruvengadam, P., Indu, J., and *Ghosh, S.*, 2020: Significance of 4DVAR Radar Data Assimilation in Weather Research and Forecast Model-Based Nowcasting System. *Journal of Geophysical Research: Atmospheres*, *125*, 1–20. https://doi.org/10.1029/2019JD031369

Tiwari, G., and *Kumar, P.*, 2022: Predictive skill comparative assessment of WRF 4DVar and 3DVar data assimilation: An Indian Ocean tropical cyclone case study. *Atmospheric Research*, *277*. https://doi.org/10.1016/j.atmosres.2022.106288

Trémolet, Y., 2006: Accounting for an imperfect model in 4D-Var. *Quarterly Journal of the Royal Meteorological Society*, *132*. https://doi.org/10.1256/qj.05.224

Trenberth, K.E., 2005: The Impact of Climate Change and Variability on Heavy Precipitation, Floods, and Droughts, In: Encyclopedia of Hydrological Sciences. https://doi.org/10.1002/0470848944.hsa211

UCAR, 2015a: NCEP GDAS/FNL 0.25 Degree Global Tropospheric Analyses and Forecast Grids.

UCAR, 2015b: NCEP GFS 0.25 Degree Global Forecast Grids Historical Archive.

Vourlioti, P., Mamouka, T., Agrafiotis, A., and *Kotsopoulos, S.*, 2022: Medicane Ianos: 4D-Var Data Assimilation of Surface and Satellite Observations into the Numerical Weather Prediction Model WRF. *Atmosphere*, *13*. https://doi.org/10.3390/atmos13101683

Wang, Y., Li, X., and *Chen, Y.*, 2023: Combined assimilation of hourly rainfall data and every 10-min AHI radiance with WRF 4DVar for the short-range heavy rainfall forecast in Eastern China. *Atmospheric Research*, *292*. https://doi.org/10.1016/j.atmosres.2023.106867

Wu, Y., Liu, Z., and *Li, D.*, 2020: Improving forecasts of a record-breaking rainstorm in Guangzhou by assimilating every 10-min AHI radiances with WRF 4DVAR. *Atmospheric Research*, *239*. https://doi.org/10.1016/j.atmosres.2020.104912

Xie, Y., Shi, J., Fan, S., Chen, M., Dou, Y., and *Ji, D.*, 2018: Impact of radiance data assimilation on the prediction of heavy rainfall in RMAPS: A case study. *Remote Sensing*, *10*. https://doi.org/10.3390/rs10091380

Yamanaka, M.D., 2016: Physical climatology of Indonesian maritime continent: An outline to comprehend observational studies. *Atmospheric Research*, *178–179*, 231–259. 10.1016/j.atmosres.2016.03.017

Yi, L., Zhang, W., and *Wang, K.*, 2018: Evaluation of heavy precipitation simulated by the WRF model using 4D-Var data assimilation with TRMM 3B42 and GPM IMERG over the Huaihe River basin China. *Remote Sensing*, *10*. https://doi.org/10.3390/rs10040646

Yulihastin, E., Nuryanto, D.E., Trismidianto, and *Muharsyah, R.*, 2021: Improvement of heavy rainfall simulated with sst adjustment associated with mesoscale convective complexes related to severe flash flood in luwu, sulawesi, indonesia. *Atmosphere*, *12*. https://doi.org/10.3390/atmos12111445

Zhang, C., Wang, Y., and *Hamilton, K.*, 2011: Improved representation of boundary layer clouds over the southeast pacific in ARW-WRF using a modified tiedtke cumulus parameterization scheme. *Monthly Weather Review*, *139*, 3489–3513. https://doi.org/10.1175/MWR-D-10-05091.1

Zhang, J., Lin, L.F., and *Bras, R.L.*, 2020: Effect of logarithmically transformed IMERG precipitation observations in WRF 4D-Var data assimilation system. *Water (Switzerland)*, *12*, 1–12. 10.3390/w12071918

Zheng, H., Chen, Y., Zheng, S., Meng, D., and *Sun, T.*, 2023: Radar Reflectivity Assimilation Based on Hydrometeor Control Variables and Its Impact on Short-Term Precipitation Forecasting. *Remote Sensing*, *15*. 10.3390/rs15030672

Zhu, H., Wheeler, M.C., Sobel, A.H., and *Hudson, D.*, 2014: Seamless precipitation prediction skill in the tropics and extratropics from a global model. *Monthly Weather Review*, *142*. https://doi.org/10.1175/MWR-D-13-00222.1